Final Report of AFOSR Project

”Study of Equatorial Ionospheric Irregularities with ROCSAT-1/IPEI Data for Assessment of Impacts on Communication/Navigation System (□)”

AOARD-05-4083

PI : Chao Han Liu

CoPI: Shin-Yi Su

National Central University

Chung-Li, Taiwan, R. O. C

May 31, 2006

Report Documentation Page

Form Approved
OMB No. 0704-0188

1. REPORT DATE	2. REPORT TYPE	3. DATES COVERED
22 SEP 2006	**Final Report (Technical)**	**01-06-2005 to 01-12-2005**

4. TITLE AND SUBTITLE
Study of Equatorial Ionospheric Irregularities with ROCSAT-1/IPEI Data for Assessment of Impacts of Communication/Navigation System (IV)

5a. CONTRACT NUMBER
FA520905P0497

5b. GRANT NUMBER

5c. PROGRAM ELEMENT NUMBER

6. AUTHOR(S)
Chao-Han Liu

5d. PROJECT NUMBER

5e. TASK NUMBER

5f. WORK UNIT NUMBER

7. PERFORMING ORGANIZATION NAME(S) AND ADDRESS(ES)
National Central University,Institute of Space Science,Chung-Li 320,Taiwan,TW,320

8. PERFORMING ORGANIZATION REPORT NUMBER
AOARD-054083

9. SPONSORING/MONITORING AGENCY NAME(S) AND ADDRESS(ES)
The US Resarch Labolatory, AOARD/AFOSR, Unit 45002, APO, AP, 96337-5002

10. SPONSOR/MONITOR'S ACRONYM(S)
AOARD/AFOSR

11. SPONSOR/MONITOR'S REPORT NUMBER(S)
AOARD-054083

12. DISTRIBUTION/AVAILABILITY STATEMENT
Approved for public release; distribution unlimited

13. SUPPLEMENTARY NOTES

14. ABSTRACT

Two major topics are studied during the first year of the two-year (2005-2007) project. The first one is the comparative study of radiowave scintillation simulations carried out with two different approaches at two different Institutions: The numerical simulation with the elliptical wave equation carried out by NCU versus the numerical solution of the thin phase-screen model carried out by AFRL/VSBXI. Although AFRL/VSBXI has sent us detailed density irregularity profile at every 50 km downward from 600 km altitude where the density structure is taken from ROCSAT-1 measurement, we were unable to make good comparison with our numerical solutions at various designated altitudes because the AFRL simulated density profile does not contain the horizontal structure to have a proportional value to the measured density structure at 600 km but has a known PSD in density fluctuation with random phase. This makes comparison difficult. However, we have tuned our numerical simulation model to have an excellent agreement with the AFRL results and with single-phase or multi-phase screen results of N. Rogers from UK. Detailed comparison will be continued during the second half of the project years. The second major accomplishment is to have a detailed analysis of the statistical distribution of the midlatitude density irregularities together with case study of midlatitude irregularity characteristics and causes. The result of the case study has been written into a paper ready for submission to publish in Journal of Geophysical Research in Space Physics in July, 2006

15. SUBJECT TERMS
Atmospheric Chemistry, Atmospheric Science, Ionospheric Irregularities

16. SECURITY CLASSIFICATION OF:			17. LIMITATION OF ABSTRACT	18. NUMBER OF PAGES	19a. NAME OF RESPONSIBLE PERSON
a. REPORT **unclassified**	b. ABSTRACT **unclassified**	c. THIS PAGE **unclassified**		**45**	

Standard Form 298 (Rev. 8-98)
Prescribed by ANSI Std Z39-18

Summary

Two major topics are studied during the first year of the two-year (2005-2007) project. The first one is the comparative study of radiowave scintillation simulations carried out with two different approaches at two different Institutions: The numerical simulation with the elliptical wave equation carried out by NCU versus the numerical solution of the thin phase-screen model carried out by AFRL/VSBXI. Although AFRL/VSBXI has sent us detailed density irregularity profile at every 50 km downward from 600 km altitude where the density structure is taken from ROCSAT-1 measurement, we were unable to make good comparison with our numerical solutions at various designated altitudes because the AFRL simulated density profile does not contain the horizontal structure to have a proportional value to the measured density structure at 600 km but has a known PSD in density fluctuation with random phase. This makes comparison difficult. However, we have tuned our numerical simulation model to have an excellent agreement with the AFRL results and with single-phase or multi-phase screen results of N. Rogers from UK. Detailed comparison will be continued during the second half of the project years.

The second major accomplishment is to have a detailed analysis of the statistical distribution of the midlatitude density irregularities together with case study of midlatitude irregularity characteristics and causes. The result of the case study has been written into a paper ready for submission to publish in Journal of Geophysical Research in Space Physics in July, 2006.

1. NCU Numerical Simulation Model of Scintillation Result and Comparison with Phase Screen Model

M. Starks of AFRL has calculated the scintillation S_4 indices for radiowave frequencies at 244, 1537 and 4100 MHz with density irregularity measurement by ROCSAT-1 on March 19, 2001 over the Ascension Island. The result is shown in Figure 1. For comparison, a UK model [N. Rogers] calculation with GPS L1 signal propagating vertically down through ionosphere with the same irregularity data using a single-phase screen or multiple-phase screen model. The calculation is simply to obtain the scintillation S_4 index with a thin phase-screen model. The result is shown in Figure 2. The solid line is for the single phase screen located at 320 km altitude, while the dashed line is using multiple phase screens at 10 km intervals between 200 and 600 km. No difference is noted for major features in S_4 indices between the two approaches at 1537 MHz. However, the AFRL model result indicates extremely large S_4 value at 244 MHz, even when the density irregularity structure is small.

Figure 3 then shows the results of NCU simulation result from solving the parabolic equation. The S_4 indices for these different frequencies are shown in the figure for comparison. First, we notice that the NCU model results are in excellent agreement with the S_4 indices at frequencies of 1537 and 4100 MHz from phase screen models in Figures 1 and 2. All major and minor features are reproduced correctly. However, for S_4 at frequency 244 MHz, noticeable difference exists. For one thing, the S_4 index from AFRL model never decreases below 0.6, a value seems too high to be realistic, unless it is a case of strong scattering for which the theoretical model is not applicable. For the observed density irregularity structure, NCU model still produces a S_4 index at 244 MHz below 0.6 in many locations. This differences in these models will be further investigated in the coming year.

ROCSAT Pass E0780000 S4 comparisons

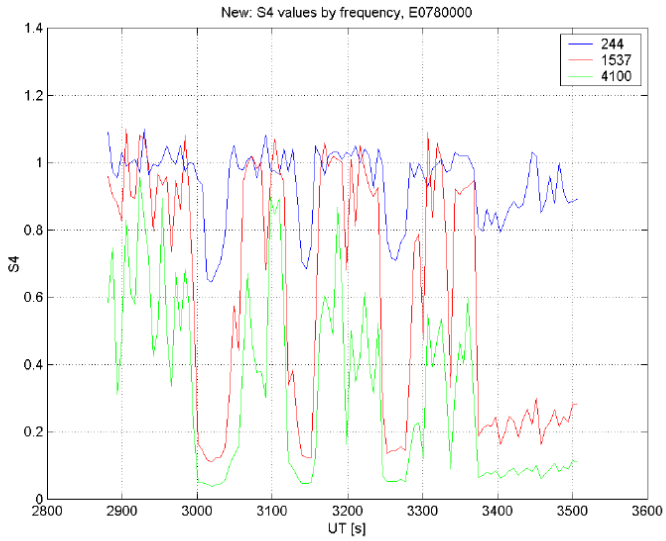

- S4 calculations at 244, 1537 and 4100 MHz (M. Starks, AFRL)
- Model calculates dN/N from ROCSAT data and assumes constant through entire ionosphere
- Ionosphere density profile derived from a Chapman profile fitted to digisonde data at Ascension Island

Fig. 1.

1.575 MHz S4 using single & multiple phase screens (N. Rogers, UK)

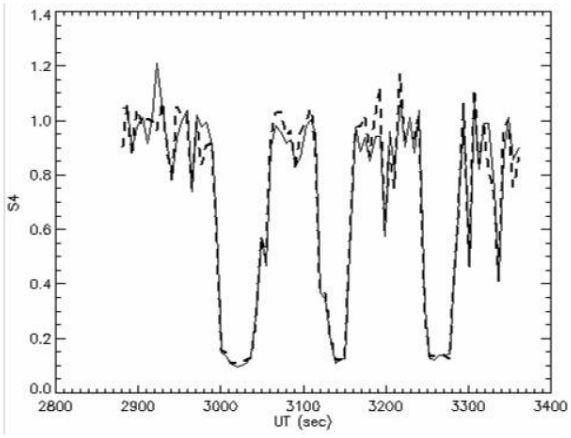

- _____ = single phase screen (summed Ne at 320km altitude)
- _ _ _ _ _ = multiple phase screens (10km intervals, 200-600km)
- Figure 1: Predicted S4 on a GPS L1 signal propagated vertically down through ionosphere determined by ROCSAT-1 measurements and the AFRL Discretized Irregularity Model for 19/3/01. The central ¾ of the phase screens of length 6656m (=1024*6.5m) was used to generate S4, which is appropriate to a 60s time series with effective IPP scan speed of 83m/s (cf. GPS scan speed of 61m/s).

Fig. 2

S4 index obtained with 4096 samples by parabolic equation method

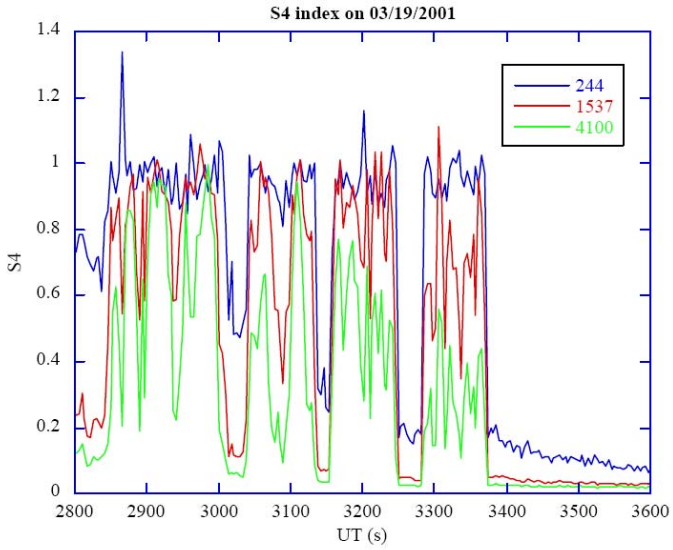

Fig. 3

2. Analysis of Statistical Occurrence Pattern of Midlatitude Density Irregularities

A detailed analysis of the statistical distribution of the midlatitude density irregularities has been carried out to understand why the AFRL wide-band scintillation map (Figure 4) does not include any existence of high occurrences of scintillation at midlatitudes. The reason could be that the roughness of the midlatitude density irregularity structure is too small to cause major concern of radiowave scintillation. The midlatitude density irregularity structure has been noted not as rough as the density irregularity structure in the equatorial and low latitude regions. As the roughness of the density irregularity structure is proportional to the severity of scintillation, the wide-band scintillation map must have set a certain threshold that happens to exclude milder density irregularity structures which populate in the midlatitude. This thought can be proved from results seen in the following four figures (Figure 5 to Figure 8). Figures 2 to 4 show the global map of the longitudinal/seasonal variation of density irregularity occurrence probability distribution. The probability of occurrence in distribution map shrinks as seen from Figure 5 to Figure 6, then to Figure 7 when the roughness of the density irregularity that is represented by the density fluctuation variance sigma value increases from 0.3% to 0.5%, then to 0.1%, respectively. This implies that the sever radiowave scintillation will also decrease accordingly and is confined to the mapped region in Figure 7. Figure 8 then summarizes the latitudinal distribution which indicates that the midlatitude irregularity indeed diminishes rapidly as the roughness of the density irregularity is concerned. Thus the AFRL wide-band scintillation map (Figure 4) thus adequately represents a good scintillation map for wide-band communication.

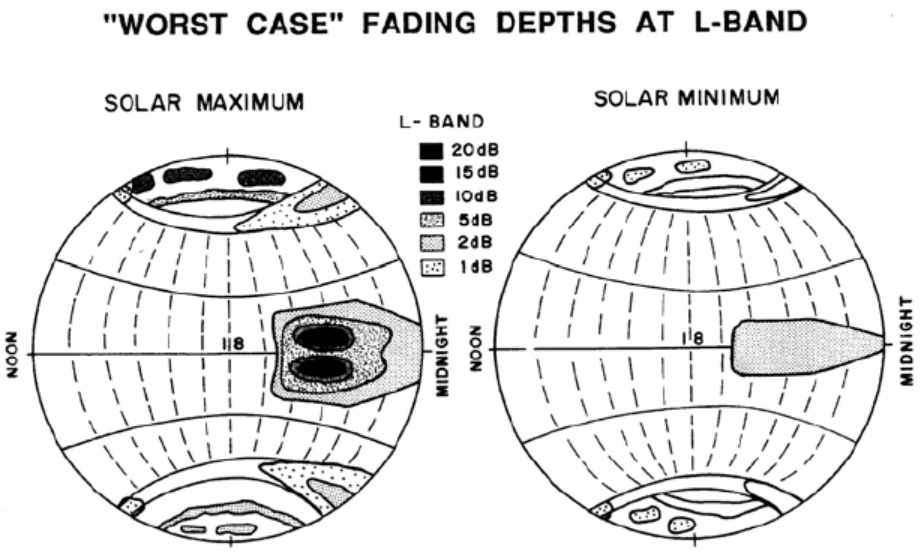

From S. Basu (2003 CEDAR Presentation)

Fig. 4 AFRL Wide-Band Scintillation Map

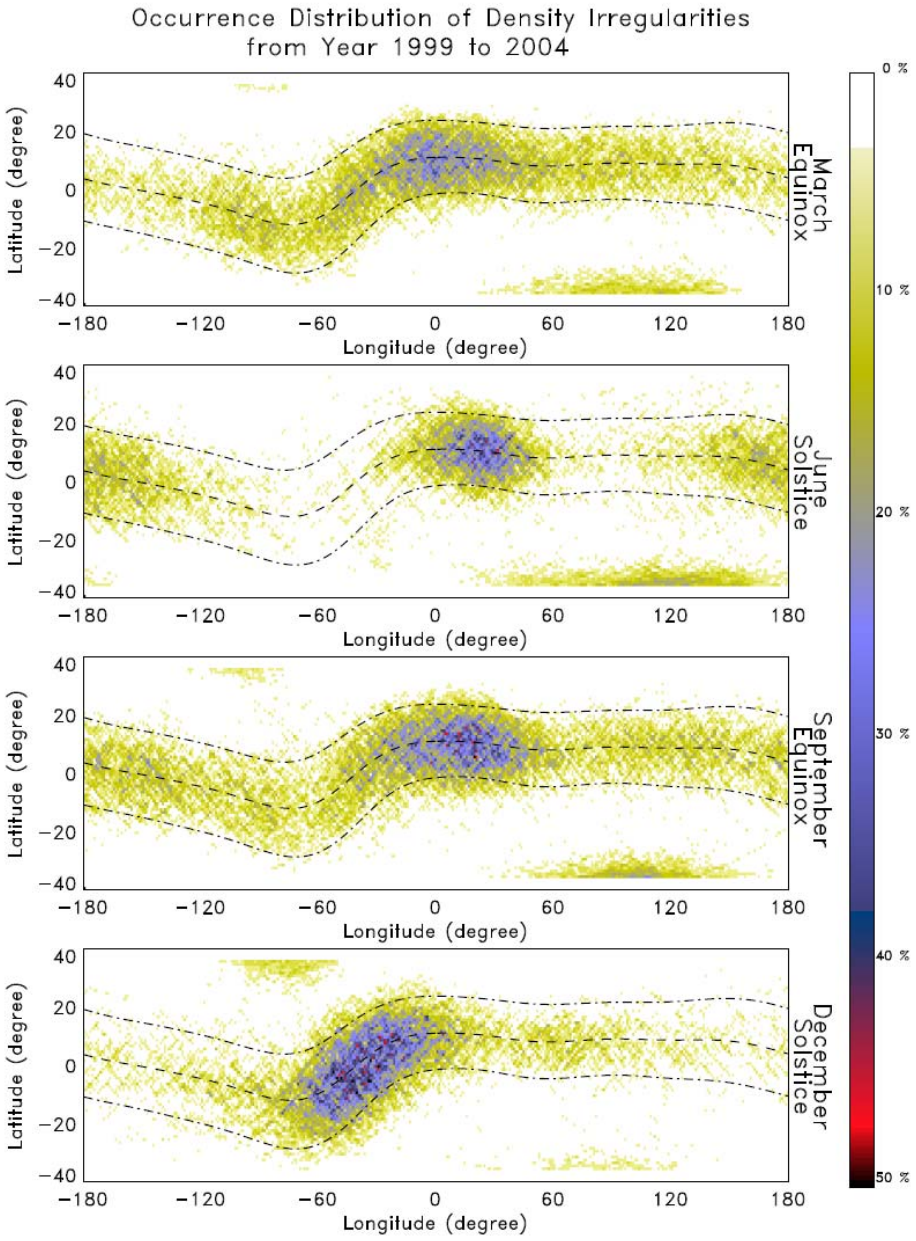

Fig. 5 ROCSAT observation of global longitudinal/seasonal distribution of ionospheric density irregularity occurrences. The threshold of density irregularity is set with $\sigma \geq 0.3\%$

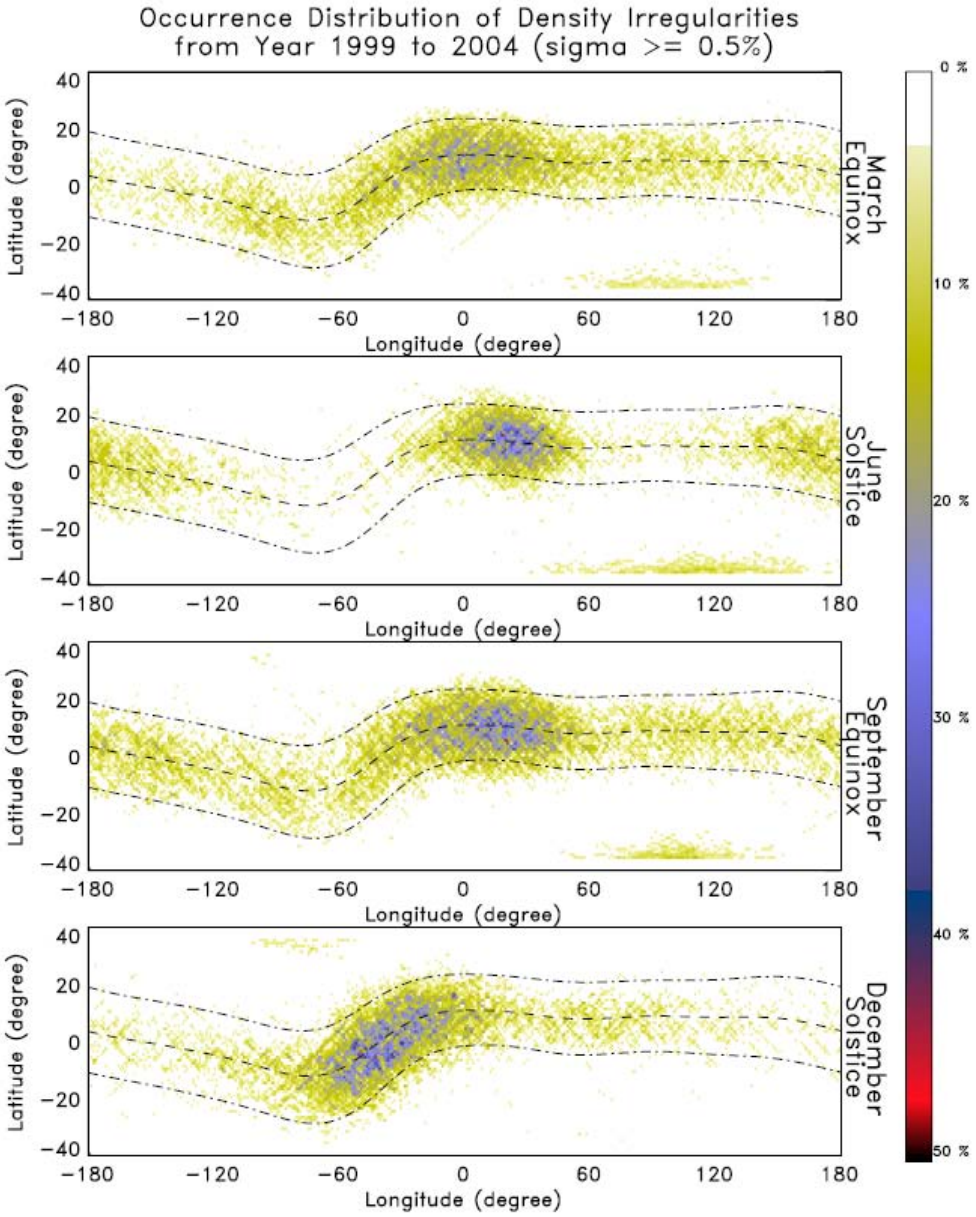

Fig. 6 ROCSAT observation of global longitudinal/seasonal distribution of ionospheric density irregularity occurrences with $\sigma \geq 0.5\%$ for rougher irregularity structure.

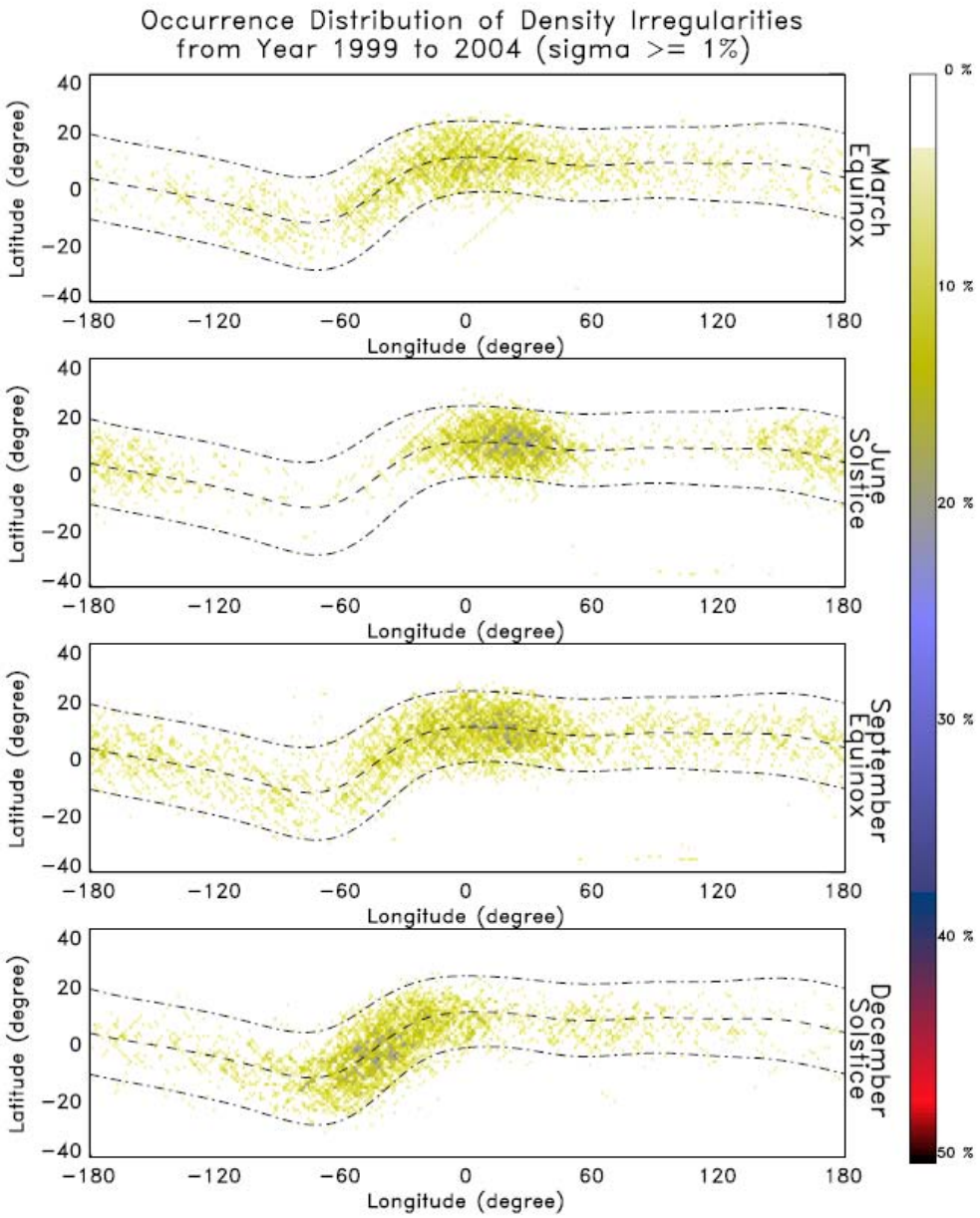

Fig. 7 ROCSAT observation of global longitudinal/seasonal distribution of ionospheric density irregularity occurrences with $\sigma \geq 0.1\%$ for very rough irregularity structure.

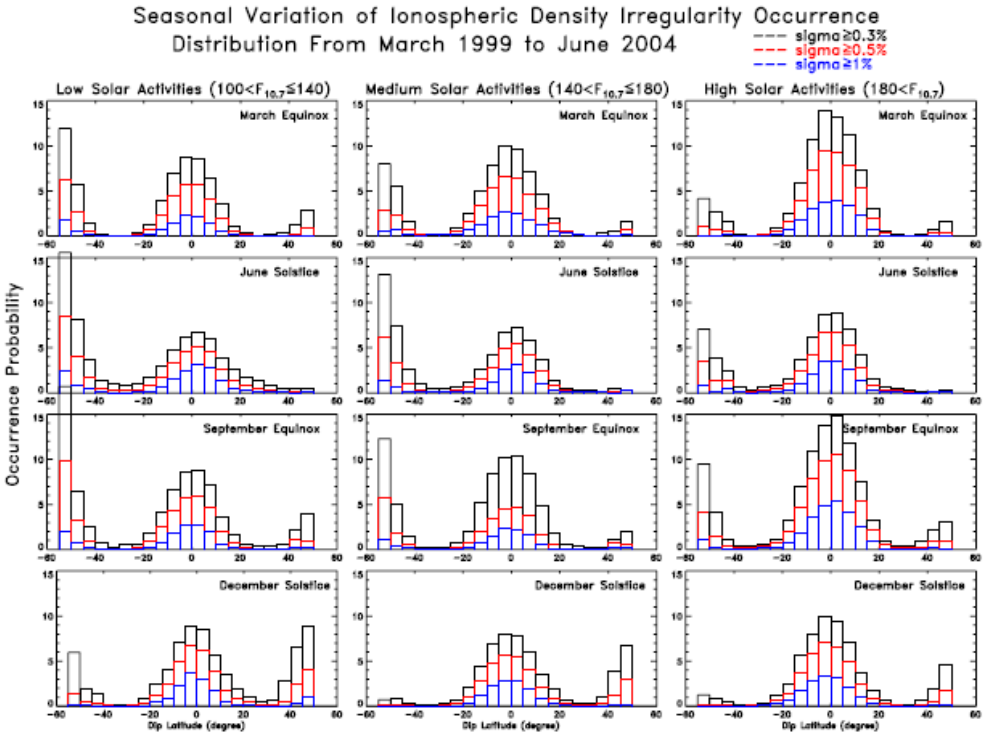

Fig. 8 The latitudinal distribution of the occurrence rate of density irregularity structures with roughness indicator of $\sigma \geq 0.3\%$, $\sigma \geq 0.5\%$ and $\sigma \geq 1.0\%$.

3. Case Study of Midlatitude Density Irregularity Events

A case of midlatitude density irregularity events observed by ROCSAT-1 on January 8, 2000 has been studied in detail for cause mechanism of midlatitude irregularities. It is found that midlatitude density irregularities of different scale sizes can occur together concurrently or alone in space and time. It turns out that in the past, we have only studied the density irregularity at intermediate-scale of 0.1 to 50 km sizes. The scale sizes of midlatitude irregularities span into two different scale lengths in this studied event, i.e., meso scale (50 to 500 km) and intermediate-scale (0.1 to 50 km). The occurrence morphologies as well as the causes are all different for different each scale sizes. The meso-scale irregularity occurs at low midlatitudes (20° to 30° dip latitude) and is caused by the Perkins instability. While the intermediate-scale irregularity occurs at higher midlatitudes (>30° dip latitude) and seems to be related to the E region instability that can not be observed ROCSAT at 600 km altitude. This needs to be further investigated with coordinated observation of E region data.

A completed paper is enclosed herewith as an Appendix. The paper will be submitted for publication in Journal of Geophysical Research in Space Physics in July, 2006.

Appendix

ROCSAT Observations of Meso-Scale Density and Flow Undulations in Conjunction with Intermediate-Scale Density Irregularities at Midlatitude Topside Ionosphere

S.-Y. Su[1], R. T. Tsunoda[2], C. H. Liu[3],
C. K. Chao[4], J. M. Wu[4], and H. H. Ho[4]

1. Institute of Space Science, and Center for Space and Remote Sensing Research, National Central University, Chung-Li, Taiwan.
2. Center for Geospace Studies, SRI International, Menlo Park, California, U. S. A.
3. Department of Communication Engineering, and Institute of Space Science, National Central University, Chung-Li, Taiwan.
4. Institute of Space Science, National Central University, Chung-Li, Taiwan.

Index: 2443 Midlatitude ionosphere, 2439 Ionospheric irregularities
2481 Topside ionosphere, 2437 Ionospheric disturbances

Abstract

ROCSAT-1 orbiting at 600 km topside ionosphere frequently observes meso-scale (~50 to 1000 km) ion density and flow undulations at low- to mid-latitudes. During the 8 January 2000 event, noticeable intermediate-scale (0.1 to 50 km) density irregularities were also observed at midlatitudes in conjunction with the meso-scale density and flow undulations in many consecutive orbits. These meso-scale undulations indicate in-phase variations among the westward and radial outward flows, and the density enhancement. For the meso-scale undulations in the first four consecutive ROCSAT orbits, the induced electric field perturbations all point to the northeast direction at about 45° in azimuth. This implies that the meso-scale disturbance should have a frontal structure that is aligned from northwest to southeast in geographic coordinate. Since the onset of the undulation is preceded by a sudden enhancement of additional background southeast flow which can be induced by a southwest electric field, the cause of the meso-scale undulation is identified as the Perkins instability [Perkins, 1973]. As for the intermediate-scale density irregularities, no coherent phase relationship is found between the density fluctuations and the flow variations in the kilometer scales. The cause of the intermediate-scale irregularity can be explained as a result from a secondary instability in the non-uniform density in the larger-scale irregularity when it co-exists with the meso-scale undulation. However, such energy cascading process is difficult to explain the existence of intermediate-scale irregularity that exists alone in time and space. Because the stand-alone irregularities are composed of well-developed structures of plasma depletion bubbles and plasma enhancement blobs, they are not purely thermal fluctuations but are resulted from image structures mapped along the field line from lower F region or E region. Since the observation of the source structure is not

available in the current study, the cause needs to be further investigated.

1. Introduction

Midlatitude ionospheric irregularities have long been studied with echoes in ionosondes [Bowman, 1960, 1984], by radiowave propagation in scintillation experiments [Yeh et al., 1968; Rodger, 1976], or with echoes from coherent radar observations [Behnke, 1979; Fukao et al., 1991; Haldoupis and Schlegel, 1996]. The first direct space observation was made by Atmosphere Explorer E (AE-E) in a report by Hanson and Johnson [1992]. The observed density depletions varied in phase with the radial flow motion when AE-E was located at ~260 km in the bottomside ionosphere. The observation was interpreted to be related to the Perkins instability [Perkins, 1973]. Similarly, the observations of ionospheric band-like motion by Arecibo radar [Behnke, 1979] and the F-region field-aligned irregularities (FAI) by MU radar [Kelley, 1989; Kelley and Fukao, 1991] have also been interpreted with the Perkins instability. On the other hand, the observation of midlatitude electric field fluctuations (MEFs) with Dynamic Explorer 2 (DE 2) was explained with the field-aligned current flowing between the conjugate ionospheres without resorting to any instability process [Saito et al., 1995]. Even though no clear relationship between the MEFs and the midlatitude spread F has been established in their report, it is noted that the local-time distribution of the occurrence pattern for the MEFs which peaked after midnight is very similar to the high occurrence distribution of the intermediate-scale (0.1 to 50 km) midlatitude density irregularities observed by ROCSAT-1 [Su et al., 2006].

The growth rate of the Perkins instability has long been noted to be too low to sustain any adequate growth of an instability structure to be observed in space or by ground radar. Because of lacking other viable theoretical works for the midlatitude F region irregularities, the Perkins instability has been frequently referenced for comparison with the experimental observations.

In recent years, the cause of midlatitude F region irregularities has been linked to the instability of the sporadic E layers reported in a series of papers [Cosgrove and Tsunoda, 2001, 2002, 2003; Tsunoda and Cosgrove 2001; Haldoupis et al., 2003; Tsunoda et al., 2004]. The vertical shear in the nighttime zonal neutral wind that forms the midlatitude sporadic E layers will induce instabilities that are amplified when electrodynamically coupled to F region. The growth rate of this instability has been shown to be orders of magnitude larger than that of the Perkins instability. The simulation result of the quasi-periodic structure in E region plasma blob by Hysell et al. [2002] can also be used to explain F region disturbances if the instability structure is mapped to F region along the field line. All these theoretical models of E region instability indicate a frontal structure of disturbance along the northwest-to-southeast direction, similar to the result from the Perkins instability.

Referring to these theoretical works on the instabilities in the midlatitude ionosphere, we present the ROCSAT observations of midlatitude irregularities at two different scale sizes, meso-scale (~50 to 1000 km) versus intermediate-scale (0.1 to 50 km). Irregularities of these two different scales are found to co-exist together or to occur alone in space and time. These midlatitude irregularities are not related to the decayed fossil structures of equatorial plasma bubbles or irregularities because the equatorial F region plasma irregularity structure should decay at a constant rate over a broad range of horizontal scale sizes [Hysell and Kelley, 1997]. Since ROCSAT measures the ion density, ion composition, and three flow components, the dataset provides us an ideal experimental comparison with the theoretical work for the occurrence of midlatitude irregularities. The current report will also examine if any causal relationship exists between the density irregularities of the two scales.

2. ROCSAT Observations

2.1. Meso-Scale Density and Flow Undulations

January 8, 2000 was a quiet day in geomagnetic activity (daily $\sum K_p = 10.3$ and $A_p = 5$) after several slightly disturbed days in the beginning of the month. In many ascending legs of the ROCSAT orbits in the northern hemisphere, ROCSAT observed density and flow fluctuations in regions from low to middle latitudes. Although the ROCSAT orbit is 35° inclined to the geographic equator, it can reach to ~50° in dip latitude at certain longitude regions because of the tilt and offset of the magnetic dipole axis with respect to the geographic axis. Figure 1 shows the ROCSAT observations in 1-s averaged data. Thirty minutes of data in each of eight consecutive ROCSAT orbits from 0415 UT to 1615 UT are shown in the figure. In each dataset such as the one shown in Figure 1(a), three ion flow components are shown in the top three panels. $V_\perp^M$ is the flow component perpendicular to the field line and lies in the magnetic meridian plane, positive outward. $V_\perp^Z$ is the flow component in the zonal direction, positive eastward and $V_\parallel$ is the field-aligned component. The ion concentration, ion temperature and ion composition are shown in the next three panels. The universal time (UT), local time (LT), the geographic latitude (Lat) and longitude (Lon), and the dip latitude (DLat) calculated from IGRF-2000 model are annotated in the bottom of each figure. The geomagnetic field model of IGRF-2000 has also been used to obtain the ion flow components with respect to the geomagnetic field line.

By simple eye inspection of the data in Figure 1, we notice that ROCSAT has observed many large flow and density undulation events. These events are highlighted with the vertical dotted lines drawn at some peaks of noticeable $V_\perp^M$ flow variation and across panels in each figure for easy comparison among different components of ion property. For example, around 0431 UT in Figure 1(a) or around 0745 UT in Figure 1(c), the deviation of $V_\perp^M$ from the background flow is noticed to

flow outward (upward and northward) and the deviation of $V_{\perp}^{Z}$ is westward. The densities are all enhanced during these periods. Thus a clear in-phase relationship exists among the flows and density enhancement. The increase in O^{+} component of ion density is also noted to accompany with a decrease in H^{+} as well as in He^{+}. Other ion properties such as $V_{\parallel}$ flow and ion temperature do not indicate any coherent variation. The period of peak-to-peak undulation in $V_{\perp}^{M}$ varies from ~20 s (scale length of 150 km) in Figure 1(b) to ~75 s (scale length of 760 km) in Figure 1(g). These undulation events belong to a class of meso-scale (~50 to 1000 km) irregularities. Whether these undulations are related to the harmonics of one particular fundamental mode oscillation is not clear at this point.

The local-time of these large meso-scale flow and density undulations starts from ~1100 LT and ends at 0100 LT in Figure 1(a), then delays the starting time from ~0010 LT to end at 0500 LT in Figure 1(h). In other words, the occurrence of irregularity delays progressively in local time. It is also noted that the flow undulations in the earlier orbits are one-sided to one direction only, and begin to have some oscillatory components in both directions in the later orbits. That is, only the upward (outward and northward) and westward flow fluctuations are noticed in Figures 1(a) through 1(e). The flow undulation begins to have some oscillatory upward and downward motions, as well as westward and eastward components in Figures 1(f) to 1(g). The fluctuation in Figure 1(h) is rather complicated but still seems to be oscillatory. A unidirectional flow fluctuation can be thought as if the oscillatory wave motion existed in a plasma that has a background flow motion in the southeast direction to offset the southeast component of the wave motion. Indeed, ROCSAT entered a region that indicated an enhanced southeast flow at about 0422 UT in Figure 1(a), at 0602 UT in Figure 1(b), and at 0920 UT in Figure 1(c) before observing the onset of large undulation event. Thus the existence of an extra southeast flow component that is

induced by a southwest electric field could be the cause of the meso-scale flow undulation. This will be discussed further later in the discussion section.

The magnitude of the one-sided flow undulation is rather large. It reaches to about 200 m/s in both outward and westward direction at the same time. This is equivalent to having a flow undulation amplitude of 280 m/s that is induced by an electric field of ~8 mV/m pointing to northward, downward as well as eastward at a dip latitude of around 35°. Finally, we would like to point out that the oscillation in the flow components that are observed after ~1615 UT in Figure 1(h) are artifact and are not physical. It is due to the solar photon incidents on the spacecraft when ROCSAT emerges from the nighttime ionosphere at ~1615 UT (~0545 LT) on January 8, 2000.

2.2. Intermediate-Scale Density Irregularities

Unlike the meso-scale undulations which can be identified with eye inspection of data plots, the intermediate-scale (0.1 to 50 km) density irregularities are identified from calculation of density fluctuation as was done in an earlier report by Su et al. [2006]. It is identified through an auto-search program which first linearly detrends a 10-sec data segment of density variation. A density irregularity structure is then identified if the density fluctuation deviation σ satisfies the following equation,

$$\sigma = \frac{\left[\frac{1}{10}\sum_{i=1}^{10}(\log n_i - \log n_{oi})^2\right]^{1/2}}{\frac{1}{10}\sum_{i=1}^{10}\log n_{oi}} \geq 0.3\ \%, \qquad (1)$$

where n_i and n_{oi} are the measured ion density and the linearly fitted value at the *i*th data point, respectively. The density irregularity identified by the search has a scale length between 7.5 km and 75 km based on the spacecraft velocity.

We indicate the spatial extent of the intermediate-scale density irregularity structure by two short vertical bars in the density panel in Figure 1 and labeled it with the alphabet letter I in the panel. Interesting interplay between the occurrences of the meso-scale flow and density undulations and the intermediate-scale density irregularities is noticed. In Figure 1(a) around 0434 UT or in Figure 1 (b) around 0615 UT, the intermediate-scale density irregularity is observed after observing large meso-scale flow and density undulations. In other words, the intermediate-scale density irregularity structure seems to exist alone in space and time, and after the observation of meso-scale undulation. On the other hand, in the later orbits, almost concurrent observations of small density fluctuations with the large flow and density undulations are noticed in Figures 1(d), and 1(f) through 1(h). When the occurrence location in geographic coordinate is examined for the large flow undulation events against the small density fluctuation events in Figure 1(a) through 1(h), we conclude that in the earlier ROCSAT orbits, events of large flow undulation occurs before events of small density fluctuation at a slightly lower geographic latitude as well as at a lower dip latitude in Figures 1(a) to 1(c), and 1(e). A local time separation is also noticed for the earlier occurrences of large flow undulations in comparison with the small density fluctuation events. From Figures 1(d), and 1(f) to 1(h), the location and time for the occurrence between the large flow undulation and small density fluctuation become either adjacent or concurrent. The words “alone”, “adjacent”, and “concurrent” are used to emphasize the occurrence location of the intermediate-scale irregularity relative to that of the meso-scale undulation. For any perturbation, meso-scale undulation and intermediate-scale oscillation can always mix together. When the meso-scale undulation amplitudes become relatively insignificant from simple visual inspection as seen around 0435 UT in Figure 1(a), around 0616 UT in Figure 1(b), and 0758 UT in Figure 1(c), the word “stand-alone” is then adapted to

emphasize the characteristics of these intermediate-scale irregularities. In fact, the intermediate-scale irregularities are not fund with the search of Eq. (1) inside the meso-scale undulations in these figures.

The density and flow fluctuations in the intermediate-scale structure are further examined with four minutes of 32-Hz raw data taken from 0756 to 0800 UT for the case of stand-alone density fluctuations, and from 1426 to 1430 UT for the case of concurrent density fluctuations and the results are plotted in Figures 2(a) and 2(b), respectively. The high-time resolution data of the two flow velocity components are measured in the spacecraft coordinate with V_y looking to the right of the orbital track, and V_z pointing to the nadir direction. One interesting feature is immediately noticed in the stand-alone density structure shown in Figure 2(a). It contains sections of density depletions followed by density enhancements. For most depletion features observed before 0758:30 UT, they resemble the equatorial plasma bubbles except that these bubbles are much smaller in size. For the later irregularity structure after 0758:30 UT, the density variations are in the form of density enhancements like small plasma blobs [Oya et al., 1986]. On the other hand, Figure 2(b) reveals much more complex structure in the density fluctuation when it co-exists with the meso-scale irregularities.

Although the two flow components need to be cleaned (such as removing outliers to obtain the 1-s averaged data), they still can be used to compare with the density fluctuation to study for the correlated fluctuation. It seems that only at the density depletion of bubble structure or at the density enhancement of plasma blob in Figure 2(a) that the density variation and the V_z flow indicate in-phase correlation. That is the density decrease inside the bubble is accompanied with an upward flow, or the density increase in the plasma blob is accompanied with the downward flow. This is identical to what has been observed in the meso-scale undulation. On the other hand,

for the intermediate-scale irregularity that co-exists with meso-scale undulation in Figure 2(b), no clear phase relationship seems to exist between the density and V_z flow fluctuation. Furthermore, for the kilometer-scale fluctuations in density and flow shown in either figure, no coherent phase correlation is found from a detailed examination of blow-up sections of the figure that are not shown here.

The spectral characteristics of these density irregularities are further studied with the Fourier analysis. Power spectral density (PSD) of density fluctuation for a data segment of 16 s is shown in each panel of Figure 3. Top panels in Figure 3 are from the stand-alone irregularities in Figure 2(a). We select two segments of data to represent bubble-like structure, and two segments to represent blob-like structure. The spectra from the other four data segments in the concurrent density irregularity in Figure 2(b) are shown in the bottom panels of Figure 3. For a 16-s data segment, the irregularity wavelengths between 0.47 and 120 km are studied. Contrasting spectral characteristics from the two different types of intermediate-scale density structures are clearly noticed in Figure 3. First, the stand-alone irregularity seems to be lack of oscillation wavelength shorter than ~2 km, while perturbations with oscillatory motion at such short wavelength still exist in the concurrent irregularities. Second, a dominant oscillation at wavelength of ~80 km exists in the concurrent irregularities, while for the stand-alone irregularities the dominant ones are at its harmonics of ~40 km. Third, the spectral slope for the spectrum between wavelengths 1.5 and ~15 km (0.125 to 1.25 Hz oscillations) is noticed to be steeper in the stand-alone density irregularities (upper panels) than in those obtained for the concurrent density fluctuating structures (lower panels) that co-exist with the meso-scale flow undulations. A larger spectral power at the wavelength ~50 km seen in the spectra in the lower panels of Figure 3 indicates the existence of meso-scale oscillations in Figure 2(b). No such large power exists in the spectra shown in the upper panels of Figure 3 for the

stand-alone intermediate-scale fluctuations in Figure 2(a).

The spectral index α in the PSD of f^{α} varies from between -4.0 and -2.3 in the stand-alone density irregularities and changes to flatter than -2.3 for the density irregularities that co-exist with the meso-scale flow undulations. The background noise power is about the same at around 10^{-8} (DN/N/Hz) for either type of irregularities. The PSD at the wavelength of 5 km is also noted about the same for the two groups. Thus the steeper spectral slope is resulted from the extra power in the wavelength at ~15 km for the stand-alone intermediate irregularities. The power comes from the repetitive occurrences of plasma bubble depletions and plasma blob enhancements in Figure 2(a).

For either stand-alone or concurrent irregularity structure, the wavelength for the central range of the spectrum, between ~1.5 and ~15 km, is about five times longer than what has been found in the spectrum of equatorial bottomside sinusoidal (BSS) irregularities observed by Atmosphere Explorer C and E spacecraft [Valladares et al., 1983]. The central portion of the spectrum in the BSS structure is in the range between 300 m and 3 km with spectral indices varying from -2 to -6. The BSS spectrum further indicates a roll-off in the spectrum at ~1 km wavelength. Since BSS structures are equatorial phenomena that only occur within ±15° in dip latitudes, they could not be related to the current observations of midlatitude irregularities that do not indicate any roll-off characteristics in the spectrum but have spectrum peaks at ~40 and ~80 km. On the other hand, the current midlatitude density irregularities could be related to the midlatitude MEFs observed by DE 2 satellite [Saito et al., 1995]. However, the spectra of density irregularities are somewhat flatter than what have been found in the MEFs. The spectral indices for the MEF spectra varied between -4.1 and -4.5 in the frequency range between 0.2 and 2 Hz. As the spectrum of density irregularity has been known to be flatter than that of velocity fluctuation, the values of

spectral indices for the observed intermediate-scale density irregularities seem to fall into the expected range.

2.3. Spatial Extent of the Irregularities in the Low to Mid Latitude

To have a better view of the relative locations between the occurrences of meso-scale flow and density undulations, and the intermediate-scale density fluctuations, we construct a map of the observed irregularities in the geographic coordinate in Figure 4. The horizontal projections of the induced electric field perturbations (derived from the flow perturbations) for the meso-scale undulations are plotted on the orbital track to identify the locations and the frontal structure of the meso-scale undulations. The spatial extent of the intermediate-scale density irregularities are labeled with the alphabet letter I on the track. The contours of dip latitudes are shown with the dotted lines inside the figure.

The locations of the meso-scale undulations observed by ROCSAT starts from lower dip latitude in orbit #1 (for Figure 1(a)) to a slightly higher latitude in orbit #8 (for Figure 1(h)). Some meso-scale undulations are observed in the turned-around southbound legs of the ROCSAT orbits at low latitude starting from orbit #6. In other words, ROCSAT seems to enter a region of meso-scale disturbance that has a banded structure aligned to slightly tilted in the northwest-to-southeast direction. Because ROCSAT can not extend its orbit farther northward, the northern–most boundary of the banded structure was not observed. However, the tilted frontal structure of the disturbance does exist.

The oscillatory variation of the perturbed electric fields along the track indicates a much clearer tilt, pointing to northeast direction in many earlier orbits. It should be noted that the direction of the field vector has been corrected to point to the right

azimuth direction using different scales in latitude and longitude of Figure 4. From the fact that the meso-scale disturbance has a tilted frontal structure together with fact that such meso-scale disturbance disappears before ROCSAT encountering the intermediate-scale irregularities in her first three orbits as seen in Figure 4, it seems that the region for the meso-scale disturbance is confined in a spatial band of ~3000 km wide as seen in orbits #1 to #3. It contains only a few oscillatory cycles of one-sided undulations.

The largest amplitude of the horizontal component (as shown in Figure 4) of the induced electric field varies from 2.5 to 3.4 mV/m in the first four orbits of observation. This is about the same order of MEFs observed by DE 2 [Saito et al., 1995].

The frontal line of the disturbance structure does not seem to be perpendicular to the horizontal projection of the perturbed electric field vector. This could be due to mixing of temporal and spatial observations from many different ROCSAT orbits in observation. The normal of the disturbance front is only about 3° in the azimuth direction, while the perturbed electric vector points to ~45° in the azimuth direction.

For the intermediate-scale density irregularities, they are observed at higher midlatitude regions, either poleward of or collocated with the meso-scale undulations. No frontal structure seems to exist for the intermediate-scale irregularities. This could be due to the fact that the ROCSAT orbit has already turned southbound so that no further information about the intermediate-scale irregularities at higher midlatitudes is obtained. Thus the intermediate-scale density fluctuation structures are all located at least at slightly higher dip latitudes than the meso-scale large undulations.

3. Discussion and Conclusions

Before proceed further, it should be mentioned that the observation of conjunctive

occurrences of meso-scale undulations with intermediate-scale density irregularities on January 8, 2000 is not a single incident. Many other cases of such conjunctive occurrences are observed in December 1999 through January 2000. Although January 8, 2000 is a magnetic quiet day, other cases have been observed during slightly disturbed days. The occurrences of intermediate-scale density irregularities at midlatitudes have been statistically concluded to be independent of the geomagnetic condition [Su et al., 2006]. A similar conclusion for the occurrences of meso-scale large flow undulations can be inferred from the current study.

Furthermore, it should be noted that the occurrences of intermediate-scale density irregularities are not limited to midlatitudes higher than 30° in dip latitude. The intermediate-scale density structure can occur together with an equatorial plasma bubble depletion and becomes part of large equatorial plasma bubble structure in the equatorial to low latitude regions. The latitudinal distribution of intermediate-scale density irregularities, in fact, is peaked at the dip equator and decreases to near zero at 30° in dip latitude, same as the distribution of equatorial plasma depletion structures. It then increases again toward higher midlatitudes to form a different distribution population that has opposite occurrence characteristics in comparison with the equatorial distribution. The current observation further indicates that they can either co-exist with the meso-scale flow undulations or occur alone in time and space.

From the decay pattern of an equatorial plasma depletion structure, Hysell and Kelley [1997] have shown that the irregularity structure of different scale sizes should decay at a constant rate. Therefore, it seems peculiar that intermediate-scale density irregularity structures have appeared alone in space and time as seen in Figures 1(a) through 1(c). It is curious to know if the existence of the meso-scale density flow undulation in the neighborhood could play a role to the existence of intermediate-scale density irregularities. We notice that the meso-scale irregularity is first observed at

lower midlatitude followed by the intermediate-scale strucutre which is observed at middle latitude during the earlier ROCSAT orbits before midnight. The occurrence of meso-scale irregularity then progressively moves to middle latitude to collocate with the intermediate-scale irregularity after midnight. In the latitudinal distribution, the meso-scale undulations seem to fill-in a spatial location around 30° in dip latitude that has a minimum occurrence rate for the intermediate-scale density irregularities as reported by Su et al.[2006].

The observed meso-scale density and flow undulation simply reflects the topside ionosphere motion at ROCSAT altitude. At topside ionosphere, the outward flow motion should be in phase with density enhancement because of the downward density gradient in the O^+ profile. This has been envisioned by Hanson and Johnson [1992] from their observation of the AE-E data taken at 260 km below the F peak in which the outward flow was accompanied with density decrease. Figure 1 indicates that the outward ion flow indeed results in ion density enhancement observed at 600 km topside ionosphere. In addition, the ROCSAT observation further confirmed our understanding of the vertical profiles of O^+ ion species in relation to the light ion species of H^+ or He^+ at topside ionosphere, where an increase in O^+ will accompany with a decrease in H^+ as well as in He^+ ions.

As the perturbed flow moves only radially outward (northward) without exhibiting inward (southward) and downward motion, and has only a westward motion without eastward motion, we interpreted this as the existence of an extra southwest pointed background electric field to generate a southeast additional flow that offsets the southeast component of the oscillatory flow motion. This extra southwest pointed electric field added to the background field has caused the meso-scale flow undulation. The extra westward field component will weaken the existing eastward electric field (or the equatorward neutral wind effect) that maintains the equilibrium configuration

of the midlatitude ionosphere [Perkins, 1973]. The other extra southward field component then serves to trigger the Perkins instability as reported by Kelley and Fukao [1991]. The growth rate of the instability given in their report of equation (2) as,

$$\gamma = (E_0 / BH)\cos(D)\sin^2\left(\theta/2\right) ,$$

where E_0 is the magnitude of the horizontal component of the total electric field measured in the Earth fixed frame. H is the neutral scale height. The angle D is the dip angle of the geomagnetic field $\underset{\sim}{B}$, which is about 55° in the current observation with $\left|\underset{\sim}{B}\right|$ of 3.3x10^4 nT. The angle θ is the propagation direction of the disturbance measured from east, which in the current observation is 45°. Using the observed value of $(E_0/B) \approx 250\ m/s$ for our case in Figure 1(a) and assume H = 50 km for Ox neutrals at 600 km, we obtain the growth rate of 0.24/min. This indicates the disturbance can grow e-fold in about 4 minutes. The long enough time delay before observing the meso-scale undulation in Figure 1 indicates that the Perkins instability is the cause.

When Figure 1 is examined for the background flow condition for the existence of meso-scale undulations, it is noticed that the undulations exist within a region during the inward contraction of the ionosphere with small eastward flow motion. An inward contraction or collapsing of the ionosphere has been reported to induce the kilometer scale irregularity from the Arecibo observation [Basu et al., 1981]. Besides the Perkins instability that can cause the kilometer scale irregularities, the $\underset{\sim}{E}\times\underset{\sim}{B}$ gradient drift instability has also been used to explain the scintillation observation in the report of Basu et al.. Here we did not attempt to adopt the $\underset{\sim}{E}\times\underset{\sim}{B}$ gradient drift

instability to explain the meso-scale undulation event because of larger scale sizes in the current undulation event than in their report. Another possibility for the cause of disturbance is from the instability model of sporadic E layers that will also indicate the relationship between the outward (upward) ion flow and the density enhancement. Unfortunately, no observation data E region data is available for the current report. Nevertheless, it is noted that the instability geometry in the model will exhibit a northwest-to-southeast alignment of the disturbance. In addition, the perturbation electric field vectors in the instability structure will point to northeast-southwest direction. This induced northeast-southwest pointed electric field perturbations have been illustrated in a report by Tsunoda et al. [2004]. In their Figure 4, the northeast-southwest directed perturbed electric fields can be resulted from the polarization charge accumulation in a northeast-southwest propagated frontal disturbance at the Es layer. As these spatially oscillatory electric fields are mapped along the field lines to the topside ionosphere, they will induce an $\underset{\sim}{E}\times\underset{\sim}{B}$ drift of ion motion at topside ionosphere as observed.

With the generation of meso-scale density and flow undulations, it would be logical to assume that the intermediate-scale density irregularities are resulted from an energy cascading process in a secondary instability from the meso-scale undulation structure similar to the process in the equatorial spread F event [e.g., Haerendal, 1974]. Such cascading process has also been applied to the 3-m scale midlatitude turbulent upwelling events observed by MU radar [Kelley and Fukao, 1991]. If such energy cascading process does occur and creates intermediate-scale irregularities, then no simple phase correlation should exist between the flow and density fluctuations. The kilometer structure in data in Figure 2 does not seem to show any phase correlation between the density and flow fluctuations. Therefore, the central part of

intermediate-scale irregularity structure in 1.5 to 15 km scale lengths that co-existed with the meso-scale ones as seen in Figure 2(b) could be resulted from secondary instability of energy cascading process of the meso-scale undulations.

On the other hand, the cause of the intermediate-scale irregularities that occur alone without the meso-scale undulations then becomes puzzling. We notice that there are differences existed between the intermediate-scale irregularity that stands alone in space and time, and the intermediate-scale irregularity that co-exists with the meso-scale ones. The spectrum of the stand-alone irregularity has a steeper spectral slope between 1.5 and 15 km range than that of the co-existed one as seen in Figure 3. Furthermore, the stand-alone irregularities are always observed at latitudes higher than the ones that co-exist with the meso-scale undulations. In addition, the background zonal flow during the observation of the stand-alone irregularities is always westward as seen in Figures 1(a) to 1(c), in contrast to the preceding meso-scale ones that are observed when the zonal flow is eastward. When the intermediate-scale irregularity is found to co-exist with the meso-scale one in Figure 1(f) to 1(g), the background zonal flow is just reversing from eastward to westward. It is not clear at this point if the existence of a westward zonal flow during the observation of the stand-alone intermediate-scale irregularity is needed to support the existence of stand-alone irregularities. However, it should be emphasized that the stand-alone irregularity has indicated a well developed structure as seen in Figure 2(a) so that it can not be in the initial stage of an instability process. It should be a result at the final stage of an instability process. It just happens to be observed at topside ionosphere. Furthermore, it should be emphasized that it is not a fossil structure from the decaying equatorial plasma bubble structure expanded to midlatitude because it contains well-structured plasma blobs that seldom exist in the equatorial irregularity structures.

Observation of long-lasting small irregularities has been reported in the literature.

It is the equatorial bottomside sinusoidal (BSS) irregularity with a central scale sizes between 300 m and 3 km [Valladares et al., 1983]. The observation of BSS is thought to be the prelude to the excitation of equatorial Rayleigh-Taylor (R-T) instability. For a long-existing BSS that fails to evolve fully into the R-T instability is due to the damping effect of coupling the perturbed electric field to high conducting E region [Cragin et al., 1985]. Therefore, the existence of the stand-alone irregularity in the current observation could be resulted from to the mapped perturbed electric field from E region or lower F region through some instability process in that region. Mapping of kilometer size electric field from E to F region should have no difficult [Heelis and Vickrey, 1990]. Thus it is conjectured that the stand-alone intermediate-scale midlatitude irregularity is an image structure mapped from E region through an instability process of the sporadic E layers described in the models of Hysell et al. [2002], Haldoupis et al. [2003], and Tsunoda et al. [2004]. The mapped electric field creates structures of plasma bubble depletions and plasma enhancement blobs that exhibit in-phase motions in density and flow fluctuations at topside ionosphere.

In conclusion, quiettime density irregularities have been observed in several consecutive ROCSAT orbits traversing the nighttime ionosphere from 22 LT to 06 LT. The meso-scale density irregularities are observed to accompany with large flow undulations. A northwest-to-southeast frontal alignment of the meso-scale flow and density undulation is noticed for the disturbance structure. The region for the disturbances seems to be confined in band of ~3000 km wide that is aligned in the northwest-to-southeast direction. The in-phase undulation of the outward flow, the westward flow, and the density enhancement agrees with a model prediction of the Perkins instability. A sudden enhancement of the downward (southward) flow before the observation of meso-scale undulation event causes the onset of the instability. Besides the meso-scale flow and density undulation, intermediate-scale density

irregularity is also found in the same orbit either to occur alone in the proximity of the meso-scale undulation or to collocate with the meso-scale undulation. There are no phase correlation existed between the density and flow fluctuations in the kilometer-size irregularity structure. This implies that the intermediate-scale irregularity could be produced from the energy cascading process in the meso-scale irregularities when it co-exists with the meso-scale irregularity. As for the intermediate-scale irregularity that exists alone in space and time, it should be the image structure mapped from E or lower F regions resulted from some instability process. However, detailed theoretical investigation is not provided in the current report. It is hope that the current observations can serve aid to the future theoretical study of the midlatitude intermediate-scale and meso-scale irregularities.

Acknowledgement

The report is completed with a support in part from NSC94-2111-M-008-026-AP5 from National Science Council of the Republic of China, and in part, by a grant from Asian Office of Aerospace Research and Development (AOARD) of U. S. Air Force Office of Scientific Research (AFOSR), AOARD-05-4083. The ROCSAT data is processed under the support of 95-NSPO(B)-IPEI-FA07-01 from National Space Organization of the Republic of China. We also like to acknowledge the great the data processing effort of the NCU/IPEI team for the ROCSAT dataset collected between 1999 and 2004. SYS acknowledges fruitful discussion with R. A. Heelis.

References

Basu, Su., S. Basu, S. Ganguly, and J. A. Klobuchar, Generation of kilometer scale irregularities during the midnight collapse at Arecibo, J. Geophys. Res., 86, 7607-76-16, 1981.

Behnke, R. A. F layer height bands in the nocturnal ionosphere over Arecibo, J. Geophys. Res., 72, 8222, 1973.

Bowman, G. G., Further studies of “spread-F” at Brisbane, Planet. Space Sci. 2, 133, 1960.

Bowman, G. G., A comparison of mid-latitude and equatorial-latitude spread-F characteristics, J. Atm. And Terr. Phys., 46, 65-71, 1984.

Cosgrove, R. B. and R. T. Tsunoda, Polarization electric fields sustained by closed-current dynamo structures in midlatitude sporadic E, Geophys. Res. Lett., 28, 1455-1458, 2001.

Cosgrove, R. B. and R. T. Tsunoda, A direction-dependent instability of sporadic-E layers in the nighttime midlatitude ionosphere, Geophys. Res. Lett., 29, No.18, 1864, doi:10.1029/2002GL014669, 2002.

Cosgrove, R. B. and R. T. Tsunoda, Simulation of the nonlinear evolution of the sporadic-E layer instability in the nighttime midlatitude ionosphere, J. Geophys. Res., 180, No.A7, 1283, doi;10.1029/2002JA009728, 2003.

Cragin, B. L., C. E. Vallaradares, W. B. Hanson, and J. P. McClure, Bottomside sinusoidal irregularities in the equatorial F region, 2. Cross-correlation and spectral analysis, J. Geophys. Res., 90, 1721-1734, 1985.

Fukao, S., M. C. Kelley, T. Shirakawa, T. Takami, M. Yamameto, T. Tsuda, and S. Kato, Turbulent upwelling of the midlatitude ionosphere, 1. Observational results by the MU radar, J. Geophys. Res., 96, 3725-3746, 1991.

Haldoupis, C. and K. Schlegel, Characteristics of midlatitude coherent backscatter from the ionospheric E region obtained with Sporadic E Scatter experiment, J. Geophys. Res., 101, 13,387, 1996.

Haldoupis, C., M. C. Kelley, G. C. Hussey, and S. Shalimov, Role of unstable sporadic-E layers in the generation of midlatitude spread F, J. Geophys Res., 108, A12, 1446, doi:10.1029/2003JA009956, 2003.

Haerendal, G.., Theory of equatorial spread-F, Report, Max-Planck Institut fur Physik und Astrophysik, Munich, 1974.

Hanson, W. B. and F. S. Johnson, Lower midlatitude ionospheric disturbances and the Perkins instability, Planet. Space Sci., 40, 1615-1630, 1992.

Heelis, R. A. and J. F. Vickrey, Magnetic field-aligned coupling effects on ionospheric plasma structure, J. Geophys. Res., 95, 7995-8008, 1990.

Hysell, D. L., M. Yamamoto, and S. Fukao, Simulation of plasma clouds in the midlatitude E region ionosphere with implications for type I and type II quasiperiodic echoes, J. Geophys. Res., 107, A10, 1313. doi:10.1029/2002JA009291, 2002.

Hysell, D. L. and M. C. Kelley, Decaying equatorial F region plasma depletions, J. Geophys. Res., 102, 20,007-20,017, 1997.

Kelley, M. C., The Earth Ionosphere: Plasma Physics and Electrodynamics, Academic Press, Inc., New York, 1989.

Kelley, M. C. and S. Fukao, Turbulent upwelling of the midlatitude ionosphere, 2. Theoretical Framework, J. Geophys. Res., 96, 3747-3753, 1991.

Oya, H., T. Takahashi, and S. Watanabe, Observation of low latitude ionosphere by the impedance probe on board the Hinotori satellite, J. Geomag. Geoelectr., 38, 111-113, 1986.

Perkins, F., spread F and ionospheric currents, J. Geophys. Res., 78, 218-226, 1973.

Rodger, A. S., The simultaneous occurrence of spread-F at magnetically conjugate points, J. Atmos. Terr. Phys., 38, 1365-1368, 1976.

Saito, A., T. Iyemori, M. Sugiura, N. C. Maynard, T. L. Aggson, L. H. Brace, M. Takeda, and M. Yamamoto, Conjugate occurrence of the electric field fluctuations in the nighttime midlatitude ionosphere, J. Geophys. Res., 100, 21,439-21,451, 1995.

Su, S.-Y., C. H. Liu, H. H. Ho, and C. K. Chao, Distribution characteristics of topside ionospheric density irregularities: Equatorial regions vs. midlatitudes, in press, J. Geophys. Res., 2006.

Tsunoda, R. T. and R. B. Cosgrove, Coupled electrodynamics in the nighttime midlatitude ionosphere, Geophys. Lett., 28, 4,171-4,174, 2001.

Tsunoda, R. T., R. B. Cosgrove, and T. Ogawa, Azimuth-dependent Es layer instability: A missing link found, J. Geophys. Res., 109, A12303, doi:10.1029/2004JA010597, 2004.

Vallardares, C. E., W. B. Hanson, J. P. McClure, and B. L. Cragin, Bottomside sinusoidal irregularities in the equatorial F region, J. Geophys. Res., 88, 8025-8042, 1983.

Yeh, K. C., D. Simonich, J. Mawdsley, and G. F. Preddy, Scintillation observations at medium latitude geomagnetically conjugate stations, Radio Sci., 3, 690-697, 1968.

Figure Captions

Fig. 1. Data from portion of eight consecutive ROCSAT orbits where midlatitude density irregularities are observed are shown in eight panels, respectively.

Fig. 2. 32-Hz high resolution data of intermediate-scale density irregularity observed in the spacecraft coordinate system are shown in the figure.

Fig. 3. Fourier spectra for 16 seconds of high resolution density data in intermediate-scale are shown in each of 8 panels. The spectral index between 3 km to 30 km wavelength range from fitted line is shown inside each panel.

Fig. 4. Composite spatial extent of the midlatitude irregularities observed by the eight consecutive ROCSAT orbits.

ROCSAT-1 IPEI Observation, January 08, 2000

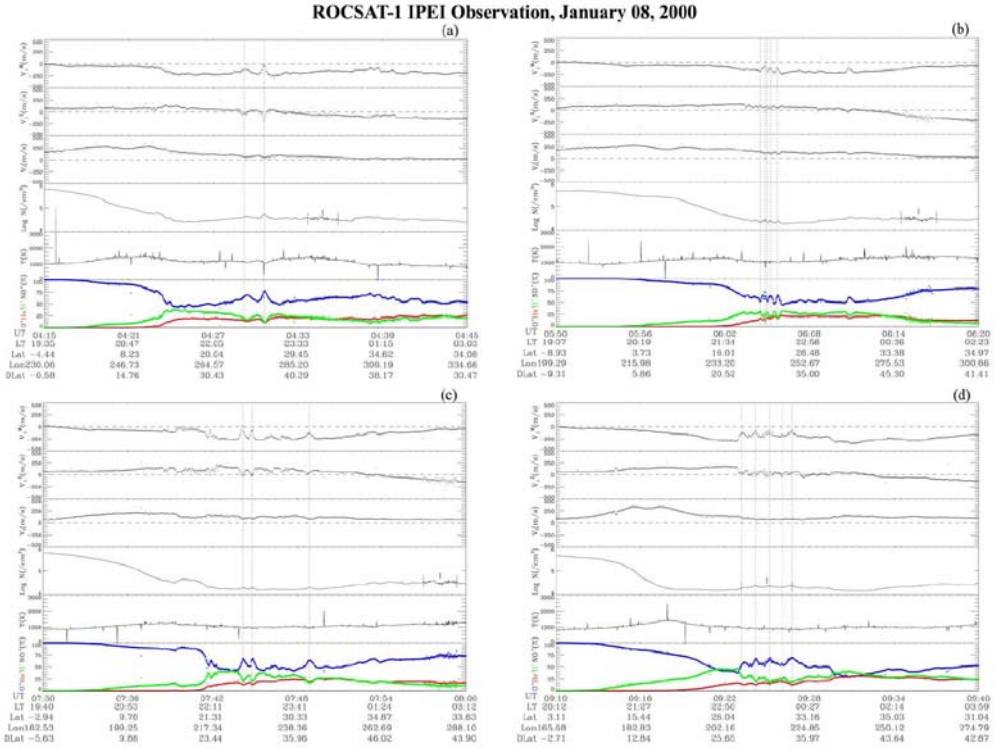

ROCSAT-1 IPEI Observation, January 08, 2000

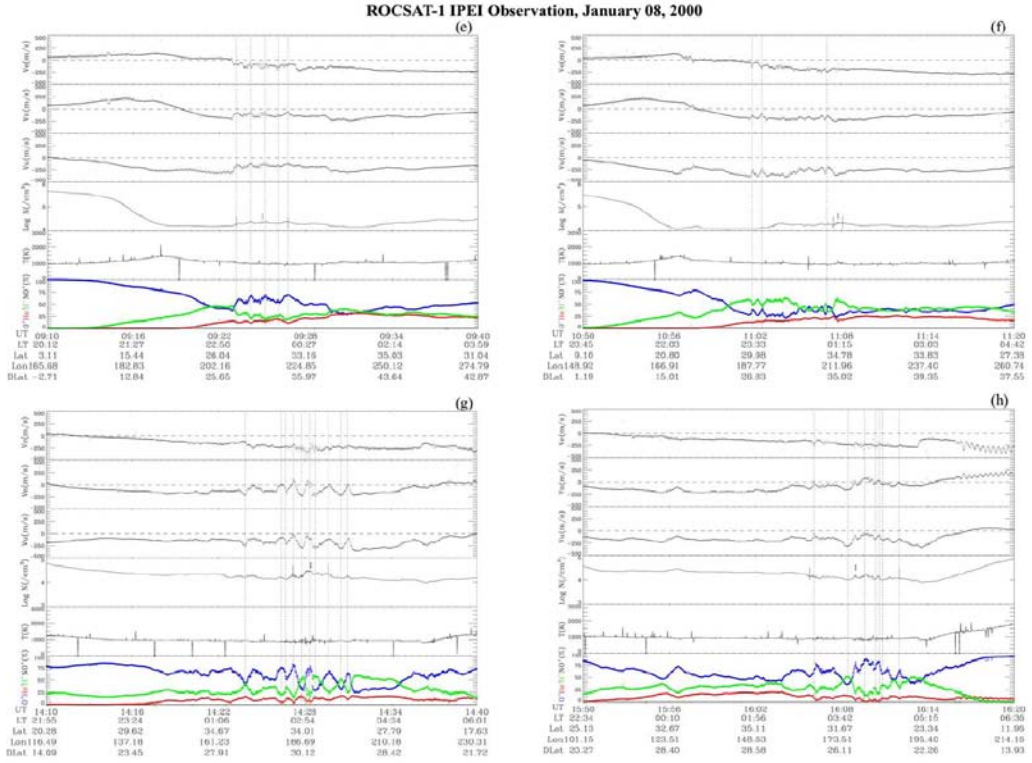

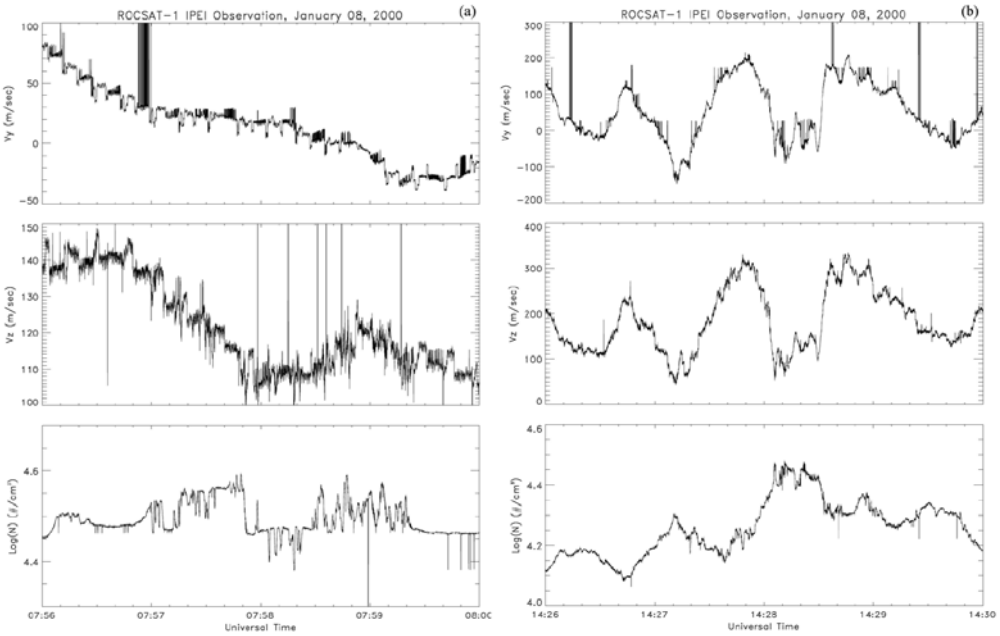
ROCSAT-1 IPEI Observation, January 08, 2000
(a)
ROCSAT-1 IPEI Observation, January 08, 2000
(b)
Vy (m/sec)
Vz (m/sec)
Log(N) (#/cm³)
Universal Time
07:56
07:57
07:58
07:59
14:26
14:27
14:28
14:29
14:30

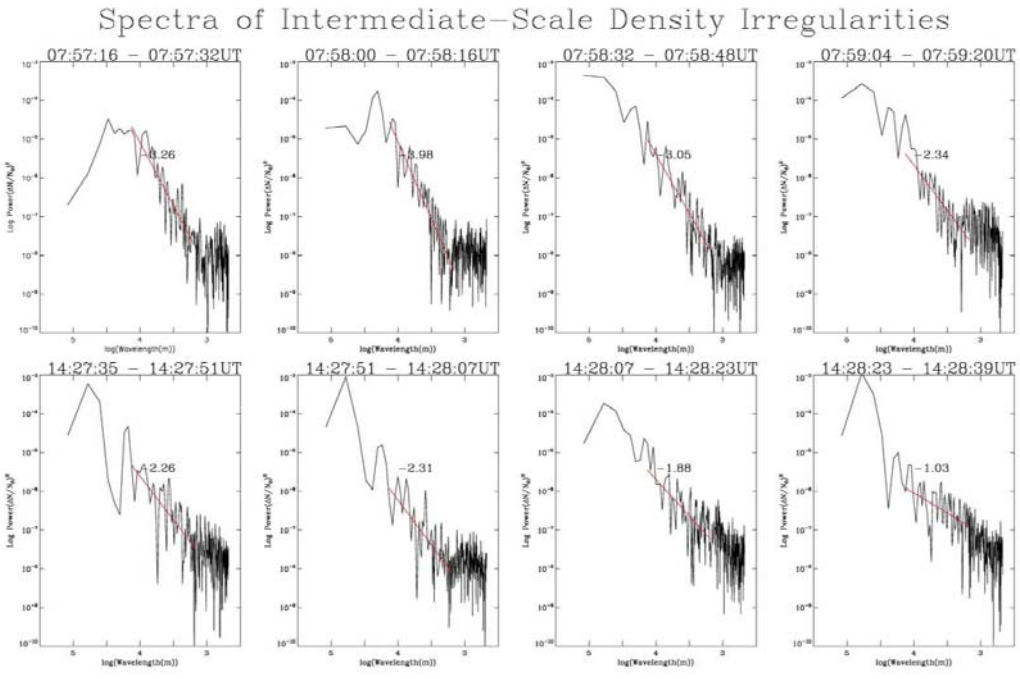
Spectra of Intermediate-Scale Density Irregularities
07:57:16 - 07:57:32UT
-3.26
07:58:00 - 07:58:16UT
-3.98
07:58:32 - 07:58:48UT
-3.05
07:59:04 - 07:59:20UT
-2.34
14:27:35 - 14:27:51UT
-2.26
14:27:51 - 14:28:07UT
-2.31
14:28:07 - 14:28:23UT
-1.88
14:28:23 - 14:28:39UT
-1.03
log(Wavelength(m))

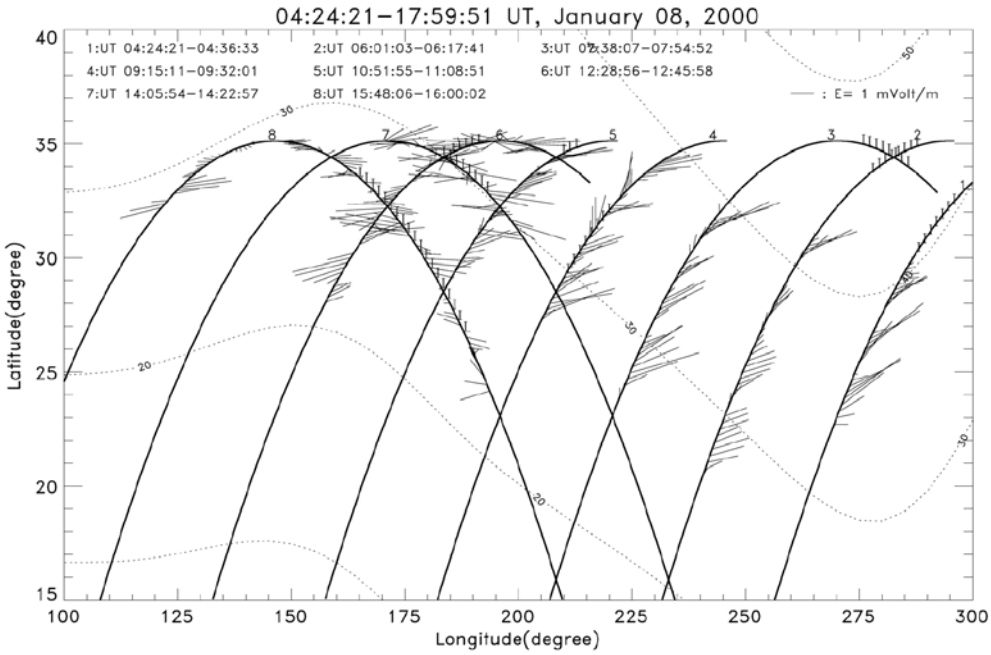
04:24:21−17:59:51 UT, January 08, 2000
1:UT 04:24:21−04:36:33
2:UT 06:01:03−06:17:41
3:UT 07:38:07−07:54:52
4:UT 09:15:11−09:32:01
5:UT 10:51:55−11:08:51
6:UT 12:28:56−12:45:58
7:UT 14:05:54−14:22:57
8:UT 15:48:06−16:00:02
: E= 1 mVolt/m
Latitude(degree)
Longitude(degree)
40
35
30
25
20
15
100
125
150
175
200
225
250
275
300